62-4-4

TRG
INCORPORATED

COMPARISON OF TWO APPROXIMATE DIPOLE DISTRIBUTIONS FOR A LENTICULAR CYLINDER IN A SEMI-INFINITE FLUID

Scientific Report No. 2
Contract No. Nonr - 2427(00)

TECHNICAL RESEARCH GROUP
2 AERIAL WAY • SYOSSET, NEW YORK

TRG, Incorporated
2 Aerial Way
Syosset, L.I., N.Y.

COMPARISON OF TWO APPROXIMATE DIPOLE DISTRIBUTIONS FOR A LENTICULAR CYLINDER IN A SEMI-INFINITE FLUID

Scientific Report No. 2
Contract No. Nonr - 2427(00)

Authors: J. Kotik
J. Kotik

V. Mangulis

Approved: J. Kotik
J. Kotik

Submitted to:
Mathematical Sciences Division
Office of Naval Research
Washington 25, D.C.

February 15, 1962

TECHNICAL RESEARCH GROUP

TABLE OF CONTENTS

ABSTRACT

Exact dipole distributions in closed form are not known for any explicitly-defined bodies in uniform translation under a free surface. Exact dipole distributions are known for some special families of bodies in uniform translation in an infinite fluid. One of these families consists of the lenticular cylinders, which are of interest in connection with ships because they can have any preassigned entrance angle. The exact and linearized dipole distributions generating lenticular cylinders in an infinite fluid are compared for various values of a fullness parameter. These dipole distributions are approximations to the exact dipole distribution generating a (vertical) lenticular cylinder in the presence of a free surface. Each of these dipole distributions has a wave resistance, the wave resistance of the linearized dipole distribution being Michell's wave resistance for the lenticular cylinder. It is found that for practical values of a fullness parameter the two approximate dipole distributions are not very close, and for Froude numbers around. .4 the wave resistances may differ by as much as 40%. This difference is larger than the uncertainty in the "measured" wave resistance, and it is proposed that experiments be conducted to determine the relative merits of the two approximate dipole distributions in predicting wave resistance. If Michell's dipole distribution for an arbitrary form is modified in an ad hoc but natural way suggested by the results for lenticular cylinders, a comparison with existing measured wave resistance can be carried out. Similar remarks apply to the asymptotic behaviour of the wave resistance at low speed.

TABLE OF NOMENCLATURE

A, cross sectional area of the cylinder

$$A_h = \frac{4\pi L}{c} \int_{-1/2}^{1/2} \sigma(x)dx = -\frac{4\pi}{c} \int_{-L/2}^{L/2} \hat{\sigma}(\hat{x})d\hat{x}$$

a, one half the width of the cylinder in the x-direction (see Figure 2)

C_w, wave resistance coefficient

C_w^{EIF}, wave resistance coefficient of the dipole distribution which represents the body exactly in an infinite fluid (and related to $f_\epsilon(x)$)

C_w^M, wave resistance coefficient of Michell's dipole distribution (and related to $g_\epsilon(x)$)

c, cylinder velocity

f, Froude number $= c/\sqrt{gL}$

$F = 1/f^2$

F_n, coefficient of $(1-4x^2)\epsilon^n$ in a power series expansion of $f_\epsilon(x)$, see Equation (10)

$$f_\epsilon(x) = -\frac{2\pi}{c}\sigma_{EIF}(x)$$

G, Green's function

G_n, coefficient of $(1-4x^2)\epsilon^n$ in a power series expansion of $g_\epsilon(x)$, see Equation (9)

g, gravitational acceleration

$g_\epsilon(x) = -\frac{2\pi}{c}\sigma_M(x)$ = the cross sectional shape of the lenticular cylinder

$h(x)$, a function proportional to a dipole distribution, such that $\int_{-1/2}^{1/2} h(x)dx = 1$.

k, radius of the circle forming the cross section of the lenticular cylinder

$L = 2a$, see Figure 1.

m, an integer greater than zero such that $mp \leq 1$

p, parameter defining the shape of the cylinder, see Figure 2.

$\hat{R}_w$, wave resistance

$\hat{R}_w^{EIF}$, wave resistance of σ_{EIF}

$\hat{R}_w^M$, wave resistance of σ_M

r, local radial coordinate, see Figure 8

$\vec{v}$, fluid velocity

w, complex velocity potential

x, y, z, normalized rectangular coordinates, see Figure 1 and Appendix B.

$\hat{x}, \hat{y}, \hat{z}$, unnormalized rectangular coordinates

$\hat{x}_m$, the x-coordinate of the m^{th} singularity in ϕ

Y_o, Bessel function of the second kind, order zero

$\hat{z}_m$, the z coordinate of the m^{th} singularity in ϕ

α, local angular coordinate, see Figure 8

ϵ, average half-beam of the shape, divided by the length, i.e., $\epsilon = A/2L^2$

$\epsilon_f = \int_{-1/2}^{1/2} f_\epsilon(x)dx$

$$\epsilon_g = \int_{-1/2}^{1/2} g_\epsilon(x)\,dx = \frac{A}{2L^2} = \epsilon$$

$$\epsilon_h = \frac{A_h}{2L^2}$$

$$\zeta = \xi + i\eta$$

η, bipolar coordinate defined by Equations (1) and (2)

μ_m, strength of the m^{th} discrete dipole source

ξ, bipolar coordinate defined by Equations (1) and (2)

$$\xi_o = \frac{p\pi}{2}$$

ρ, density

$\sigma, \hat{\sigma}$, dipole distribution; $\sigma(x) = \hat{\sigma}(\hat{x})$

σ_{EIF}, dipole distribution which is exact in an infinite fluid

σ_M, Michell's dipole distribution

ϕ, $\hat{\phi}$, velocity potential, see Appendix B

$\hat{\phi}_m$, approximate ϕ in the vicinity of the m^{th} discrete dipole source.

1. INTRODUCTION

In 1898 J.H. Michell published a paper entitled "The Wave Resistance of a Ship", in which he gave a formula for the approximate wave resistance of a thin ship[1]. It was found later[2],[3] by making a formal expansion of the complete nonlinear problem in terms of a small thickness parameter such as the beam, that Michell's formula correctly predicts the leading term in the wave resistance. The formal expansion procedure can be used to find higher-order approximations to the solution of the exact nonlinear problem but the calculations are complex and have never to our knowledge been carried out for any ship form.

Michell's result is obtained by linearizing the boundary conditions on the ship and on the free surface. If we satisfy one of these boundary conditions to a higher order than Michell did we will obtain a new approximate solution to the exact nonlinear problem. This new solution will agree with Michell (and hence be exact) to the first nonvanishing order in the thickness parameter. The second terms of Michell's solution and the new solution will disagree and both are presumably incorrect. When applied to any particular case one of these solutions will be numerically more accurate than the other. It may be that our solution is more accurate, in which case it would be useful. We cannot prove that it is, but we do show that our solution has desirable properties.

The problem of satisfying the boundary condition on the ship to higher order arises also in problems without free surface. In fact the uniform flow past a lenticular cylinder in an infinite fluid is known exactly. This exact solution and the corresponding linearized

1. INTRODUCTION

In 1898 J.H. Michell published a paper entitled "The Wave Resistance of a Ship", in which he gave a formula for the approximate wave resistance of a thin ship[1]. It was found later[2],[3] by making a formal expansion of the complete nonlinear problem in terms of a small thickness parameter such as the beam, that Michell's formula correctly predicts the leading term in the wave resistance. The formal expansion procedure can be used to find higher-order approximations to the solution of the exact nonlinear problem but the calculations are complex and have never to our knowledge been carried out for any ship form.

Michell's result is obtained by linearizing the boundary conditions on the ship and on the free surface. If we satisfy one of these boundary conditions to a higher order than Michell did we will obtain a new approximate solution to the exact nonlinear problem. This new solution will agree with Michell (and hence be exact) to the first nonvanishing order in the thickness parameter. The second terms of Michell's solution and the new solution will disagree and both are presumably incorrect. When applied to any particular case one of these solutions will be numerically more accurate than the other. It may be that our solution is more accurate, in which case it would be useful. We cannot prove that it is, but we do show that our solution has desirable properties.

The problem of satisfying the boundary condition on the ship to higher order arises also in problems without free surface. In fact the uniform flow past a lenticular cylinder in an infinite fluid is known exactly. This exact solution and the corresponding linearized

solution are discussed in Section 2, particular attention being paid to the exact and linearized dipole distributions generating these flows.

In Section 3 we use the results of Section 2 to construct a new approximate solution to the problem of a vertical lenticular strut in a uniform stream with free surface. This solution has the following properties:

1) It agrees with Michell and is therefore correct to the first nonvanishing order in the thickness parameter (for any fixed Froude number).
2) It is correct to the first nonvanishing order as the Froude number tends to zero (for any fixed thickness parameter). Michell's solution does not have this property.
3) It is correct to the first nonvanishing order as the depth of the observation point goes to infinity (for any fixed Froude number and thickness parameter). Michell's solution does not have this property.

Note that while the new solution has some properties not enjoyed by Michell's it is not claimed to be correct to higher order in the thickness parameter

In Section 4 we compute a new wave resistance for vertical lenticular struts using the new approximate solution of the flow problem. The values of wave resistance obtained by the two methods differ by as much as 40% for realistic values of the thickness parameter and for Froude numbers around .4 . This difference is larger than the uncertainty in experimentally determined wave resistance, and it is proposed that

experiments be carried out to determine the relative merits of the two approximations for predicting wave resistance. It is also shown that the new approximation leads to a different low-speed asymptotic behaviour for the wave resistance.

2. SHAPE vs. DIPOLE DISTRIBUTION FOR A LENTICULAR CYLINDER IN AN INFINITE FLUID

In an infinite fluid the cross-sectional shape $g_\epsilon(x)$ of the infinite cylinder gives the linearized dipole* distribution $-\frac{c}{2\pi} g_\epsilon(x)$. The fullness parameter ϵ is the average half-beam of the form divided by its length. The exact dipole distribution generating this shape is defined to be $-\frac{c}{2\pi} f_\epsilon(x)$. For thin bodies we expect $g_\epsilon(x) \sim f_\epsilon(x)$, in accordance with linearized theory. Since the cylinder and the fluid are assumed to be infinite, the dipole distribution is independent of the $\hat{y}$-coordinate, see Figure 1, and we can confine our discussion to the two-dimensional problem in the $\hat{x}\hat{z}$-plane, see Figures 2A, 2B.

Let us introduce the bipolar coordinates ξ, η;

$$(1) \qquad \hat{x} = \frac{a \sinh \eta}{\cosh \eta - \cos\xi}$$

$$(2) \qquad \hat{z} = \frac{a \sin \xi}{\cosh \eta - \cos\xi}$$

The shape of the lenticular cylinder (formed by the intersection of two circular cylinders) is given by $\xi = \xi_o = \frac{p\pi}{2}$. The complex potential w for such a cylinder moving in the negative $\hat{x}$-direction with velocity c (or for a stationary cylinder in a uniform stream moving in the positive $\hat{x}$-direction with velocity c) is given by[4]

$$(3) \qquad w = ica\left(\frac{2}{p} \cot \frac{\zeta}{p} - \cot \frac{\zeta}{2}\right)$$

where $\zeta = \xi + i\eta$. The velocity potential is

---

* Dipoles in an infinite fluid, without free surface.
** Relationships between normalized and unnormalized quantities are given in Appendix B.

$$(4) \qquad \hat{\phi} = ca\left(\frac{2}{p} \cdot \frac{\sinh \frac{2\eta}{p}}{\cosh \frac{2\eta}{p} - \cos \frac{2\xi}{p}} - \frac{x}{a}\right), \quad 2a = L.$$

The parameter p is related to ϵ by

$$(5) \qquad \epsilon = \frac{\pi(2-p) + \sin p\pi}{8 \sin^2 \frac{p\pi}{2}} = \frac{A}{2L^2}$$

where A is the cross sectional area of the cylinder. Figure 3 shows ϵ vs. p for $1 \leq p \leq 2$. For a circular cylinder $p = 1$ and $\epsilon = \frac{\pi}{8}$; for a strip $p = 2$ and $\epsilon = 0$. For $p < 1$ the shape of the cylinder is shown in Figure 2B.

If $0 \leq p \leq 1$ we will call the cylinder a supercircular cylinder, and if $1 < p \leq 2$ we will call it a subcircular cylinder. For a subcircular cylinder the dipole distribution is confined to the x-axis (or the xy-plane in three dimensions), while for $p < 1$ there are additional discrete dipoles on the z-axis (i.e., lines of dipoles passing through the z-axis parallel to the y-axis). In the rest of this section we discuss only subcircular cylinders, $1 < p \leq 2$; supercircular cylinders are discussed in Appendix C.

The function $f_\epsilon(x)$ is related to ϕ by

$$(6) \qquad \left.\frac{\partial \phi}{\partial z}\right|_{z=0+} = c \frac{df_\epsilon(x)}{dx}, \quad |x| \leq \frac{1}{2}.$$

Using Eq. (4) and the relationship between normalized and unnormalized potentials (see Appendix B) we find

$$(7) \qquad f_\epsilon(x) = \frac{-\frac{2}{p} \sin \frac{2\pi}{p} (1-4x^2)^{2/p}}{(1+2x)^{4/p} + (1-2x)^{4/p} - 2(1-4x^2)^{2/p} \cos \frac{2\pi}{p}}$$

and the shape is given by

$$(8) \qquad g_\epsilon(x) = \frac{1}{2}\left(\sqrt{\csc^2 \frac{p\pi}{2} - 4x^2} + \cot \frac{p\pi}{2} \right) .$$

For small ϵ we can express $f_\epsilon(x)$ and $g_\epsilon(x)$ as a power series* in ϵ,

$$(9) \qquad g_\epsilon(x) = (1-4x^2) \sum_{n=1}^{\infty} G_n(x)\epsilon^n$$

$$(10) \qquad f_\epsilon(x) = (1-4x^2) \sum_{n=1}^{\infty} F_n(x)\epsilon^n$$

where from Equations (5), (7), and (8), we find

$$G_1 = F_1 = \frac{3}{2}$$

$$G_2 = 0$$

$$F_2 = \frac{18}{\pi}\left[1 + x\ln\left(\frac{1-2x}{1+2x}\right)\right]$$

etc.

Thus if $\epsilon \to 0$ ($p \to 2$) we see that $[g_\epsilon(x) - f_\epsilon(x)] \to 0$ for fixed x, since $G_1 = F_1$. The functions $g_\epsilon(x)$ and $f_\epsilon(x)$ are shown in Figures 4-7 for ϵ = .025, .05, .1, and .3 . The fractional difference of the two functions is, for fixed x and small ϵ ,

$$\frac{g_\epsilon(x) - f_\epsilon(x)}{g_\epsilon(x)} = -\frac{12}{\pi}\left[1 + x\ln\left(\frac{1-2x}{1+2x}\right)\right]\epsilon + \cdots$$

---

* The validity of such an expansion is examined in Appendix A.

which becomes infinite for $x = \pm 1/2$, no matter how small ϵ may be. The behaviour of the functions at $x = \pm 1/2$ is also quite different:

$$(11) \qquad f_\epsilon(x) \sim -\frac{2}{p\pi^{2/p}} \sin\frac{2\pi}{p} \cdot (\pi\delta)^{2/p} \text{ as } \delta = \frac{1}{2} - x \to 0$$

$$(12) \qquad g_\epsilon(x) \sim -\frac{1}{\pi} \tan\frac{p\pi}{2} \cdot [\pi\delta] \ .$$

The difference is apparent in Figures 4-7.

3. A NEW APPROXIMATE FREE-SURFACE FLOW PAST A VERTICAL LENTICULAR CYLINDER

Suppose a lenticular cylinder is placed upright, as shown in Figure 1, in a uniform flow with linearized free surface. The dipole distribution* generating the resulting mathematically well-defined flow is unfortunately not known. The approximate flow proposed by Michell[1] and others is the one generated by the dipole distribution**

$$(13) \qquad \sigma_M(x) = -\frac{c}{2\pi} g_\epsilon(x) \quad \text{for} \quad |x| \le \frac{1}{2}, \; y \ge 0$$

where

$$z(x,y) = \pm g_\epsilon(x)$$

is the equation of the lenticular cylinder. That this is the first non-vanishing term in an expansion of the exact nonlinear solution in powers of ϵ was assumed by Michell and verified formally by Stoker and Peters[2] and Wehausen[3]. We propose the approximate flow generated by the dipole distribution

$$(14) \qquad \sigma_{EIF} = -\frac{c}{2\pi} f_\epsilon(x) \quad \text{for} \quad |x| \le \frac{1}{2}, \; y \ge 0.$$

---

* We have adopted the convention $\vec{v} = +\text{grad}\,\phi$, so that

$$G(x,y,z;x',y',z') = [(x-x')^2+(y-y')^2+(z-z')^2]^{-1/2} + \text{regular function}$$

is the velocity potential at x,y,z of a unit sink at x',y',z' in a uniform stream under a free surface, and $-\frac{\partial G}{\partial x'}$ is the potential of a unit x-directed dipole.

** Dipoles satisfying the linearized free surface condition.

To the first nonvanishing term in ϵ we have

(15) $$\sigma_M = \sigma_{EIF},$$

as we see from Eq. (13), (14) and Eq. (9), (10) et seq. Also, $\sigma_{EIF}(x)$ is exact in an infinite fluid, as suggested by the subscript EIF, in the sense that asymptotically for large y it generates the exact two-dimensional flow past the lenticular cylinder. Asymptotically for large y σ_M generates the linearized two-dimensional flow past the lenticular cylinder.

Finally, if the Froude number f tends to zero, for any fixed value of the thickness parameter ϵ, the flow defined by σ_{EIF} approaches, for $y \geq 0$, the exact two-dimensional flow past the lenticular cylinder, the positive images required to satisfy the limiting boundary condition $\frac{\partial \phi}{\partial y} = 0$ being supplied by the free-surface dipole potential. Thus the new approximate solution to the mathematically well-defined problem of a lenticular strut in a uniform flow with linearized free surface condition has advantages not enjoyed by Michell's solution to the same problem The suitability of this model for analyzing full forms may be questioned, since for finite Froude number full forms are inconsistent with small waves On the other hand the new solution becomes exact for low Froude numbers Asymptotics aside, the practical value of the new solution will be determined by the accuracy of its numerical predictions for practical forms operating at practical Froude numbers.

4 A NEW APPROXIMATE WAVE RESISTANCE FOR A VERTICAL LENTICULAR CYLINDER

Suppose we have a dipole distribution $\hat{\sigma}(\hat{x})$ on the region $|\hat{x}| \leq L/2$, $\hat{y} \geq 0$. Within the mathematically well-defined theory of flows satisfying the linearized free surface condition the wave resistance of this dipole distribution is given exactly by [5]

$$(16) \qquad \hat{R}_w = 8\pi^2 \rho F^2 \int_{-1/2}^{1/2} \int_{-1/2}^{1/2} \sigma(x)\sigma(x')Y_0(F|x-x'|)\,dx\,dx'$$

where

$\sigma(x) = \hat{\sigma}(xL)$,

ρ is the density of the fluid,

$F = \frac{gL}{c^2}$, $f = 1/\sqrt{F}$ = Froude number,

Y_0 is the Bessel function of the second kind, order zero.

If we let $\sigma(x) = \frac{c}{2\pi} \frac{A_h}{2L} h(x)$,

where

$$\int_{-1/2}^{1/2} h(x)\,dx = 1, \text{ and } A_h = \frac{4\pi L}{c} \int_{-1/2}^{1/2} \sigma(x)\,dx$$

we can introduce a wave resistance coefficient

$$(17) \qquad C_w = 4F^2 \int_{-1/2}^{1/2} \int_{-1/2}^{1/2} h(x)h(x')Y_0(F|x-x'|)\,dx\,dx'$$

in terms of which the wave resistance becomes

$$(18) \qquad \hat{R}_w = \frac{1}{2} \rho c^2 L^2 A_h^2 C_w$$

where

$$\epsilon_h = \frac{A_h}{2L^2}$$

If $g_\epsilon(x)$ defines the shape of a subcircular lenticular cylinder, then Michell's approximate dipole distribution is

(19) $$\sigma_M(x) = -\frac{c}{2\pi} g_\epsilon(x) \quad \text{for } |x| \leq \frac{1}{2},\ y \geq 0, \text{ (see Equation (13))},$$

and Michell's wave resistance $\hat{R}_W^M$ for the lenticular cylinder is obtained by substituting $\sigma_M(x)$ for $\sigma(x)$ in Equation (16). For comparison we propose the dipole distribution

(20) $$\sigma_{EIF}(x) = -\frac{c}{2\pi} f_\epsilon(x) \quad \text{for } |x| \leq \frac{1}{2},\ y \geq 0^*$$

and the corresponding wave resistance $\hat{R}_W^{EIF}$ obtained by substituting $\sigma_{EIF}(x)$ for $\sigma(x)$ in Equation (16). The properties of the dipole distribution σ_{EIF} and the corresponding flow were discussed in Section 3. We now compare $\hat{R}_W^M$ with $\hat{R}_W^{EIF}$. Since the two dipole distributions σ_M and σ_{EIF} associated with a given lenticular cylinder will have different values of A_h (or ϵ_h), we cannot compare the values of C_w, but we must compare values of $\epsilon_h^2 C_w$ (see Equation (18)), which is done in Figures 8 - 10

For Michell's dipole distribution we have

---

* EIF means Exact in an Infinite Fluid

$$\epsilon_h = \epsilon_g = \frac{1}{L} \int_{-1/2}^{1/2} g_\epsilon(x)\,dx, \qquad h(x) = \frac{1}{L\epsilon_g}\, g_\epsilon(x),$$

while for $\sigma_{EIF}(x)$ we have

$$\epsilon_h = \epsilon_f = \frac{1}{L} \int_{-1/2}^{1/2} f_\epsilon(x)\,dx, \qquad h(x) = \frac{1}{L\epsilon_f}\, f_\epsilon(x) .$$

The graphs show $\epsilon_g^2 C_w^M$ and $\epsilon_f^2 C_w^{EIF}$ vs. the Froude number f for cylinders with p = 1.905, 1.812, and 1.635. The ϵ defined in Equation (5) is ϵ_g, and

$$\epsilon_g = \epsilon_f - \frac{6}{\pi}\,\epsilon_f^2 + \cdots \tag{21}$$

Since $2L^2\epsilon_g$ is the cross-sectional area of the lenticular cylinder, while $2L^2\epsilon_f$ is the dipole moment of the distribution σ_{EIF}, the relation $\epsilon_g = \epsilon_f - \frac{6}{\pi}\,\epsilon_f^2 + \cdots$ indicates that for small ϵ_g the dipole moment exceeds the volume. This is also true for a circular cylinder [$\epsilon_g = \pi/8$, $\epsilon_f = \pi/4$]. These results are examples of a theorem of Landweber and Yih[6], which states that added mass + buoyancy = $\frac{2\pi\rho}{c}$ [dipole moment]; since the buoyancy is the density times the volume, and the added mass is positive, the dipole moment always exceeds the volume. It follows that the volumetric portion of the discrepancy, contained in ϵ_f and ϵ_g, is always in the same direction. Michell's theory tends to underestimate the wave resistance because it underestimates the volume. Over most of the Froude number range in Figures 8-10 the portion of the discrepancy contained in the C_w's is in the same direction.

Figures 8-10 reveal a considerable difference in the values of wave resistance computed by the two methods. This difference is discussed

further below. We close this section by remarking that $\hat{R}_w^{EIF}$ has the following property which follows from statements made in Section 3: To the first nonvanishing term in ϵ we have, for fixed Froude number,

$$\hat{R}_w^{M} = \hat{R}_w^{EIF} \quad , \tag{22}$$

and both are correct to this order. For fixed ϵ we would like to conclude that to the first nonvanishing term in the Froude number f, as $f \to 0$, $\hat{R}_w^{EIF}$ is correct while $\hat{R}_w^{M}$ is not, since σ_{EIF} and σ_M have the analogous properties. We have not been able to supply a derivation, since certain apparently necessary information about the manner in which σ_{EIF} becomes exact, as $f \to 0$, is not known to us. However, we can compare the asymptotic expansions of $\hat{R}_w^{M}$ and $\hat{R}_w^{EIF}$ as $f \to 0$, namely

$$\hat{R}_w^{M} \sim \frac{1}{2}\,\rho c^2 L^2 \cdot \epsilon_g^2 \cdot \frac{8f^4}{\pi} \cdot \frac{4}{3} \tan^2 \frac{p\pi}{2} \tag{23}$$

$$\hat{R}_w^{EIF} \sim \frac{1}{2}\,\rho c^2 L^2 \cdot \epsilon_f^2 \cdot \left(\frac{8f}{\pi}\right)^{8/p} \cdot \sqrt{\pi}\,\frac{\Gamma(1+\frac{2}{p})}{\Gamma(\frac{3}{2}+\frac{2}{p})} \sin^2 \frac{2\pi}{p} \tag{24}$$

These asymptotic expansions are found by methods used in [7] and described also in [3]. We can see that Equations (23) and (24) are different, but decreasingly so as $\epsilon \to 0$ ($p \to 2$). In fact if we let $p = 2(1-\eta)$, $\eta \to 0$, and expand, Equations (23) and (24) both yield

$$\frac{1}{2}\,\rho c^2 L^2 \cdot \frac{\pi^2}{36}\,\eta^2 \cdot \frac{8f^4}{\pi} \cdot \frac{4}{3}\,(\pi\eta)^2 \tag{25}$$

There is nothing to be gained by comparing Equations (23) and (24) since both are inadequate for practical Froude numbers. However, one can find the oscillatory terms which come next in the asymptotic expansions, at which point a comparison will provide valuable information.

5. CONCLUSIONS

Figures 4, 5, 6, and 7 compare $f_\epsilon = -\frac{2\pi}{c}\sigma_{EIF}$ and $g_\epsilon = -\frac{2\pi}{c}\sigma_M$ for a lenticular cylinder. Figures 4 and 5 are the most important from a practical point of view since practical values of ϵ (based on waterplane section) are in the range .025-.050*. The discrepancy in this range can be characterized as follows:

a) In the central 80% of the form $f_\epsilon(x)$ is larger than $g_\epsilon(x)$, the discrepancy being maximum at the center. The integrals are related as in Equation (21).

b) Near the ends $f_\epsilon(x)$ vanishes to a different order than $g_\epsilon(x)$, as shown in Equations (11) and (12).

Figures 8, 9, and 10 compare the wave resistance of $\sigma_{EIF}(x)$ and $\sigma_M(x)$. Figures 8 and 9 are the most interesting from a practical point of view. The numbers were computed using a digital computer program whose accuracy decreases with Froude number, and for that reason no results are presented for $f < .3$. The discrepancy in wave resistance is not small compared to typical discrepancies between calculated and measured wave resistance, and is large compared to the uncertainty in measured wave resistance. The discrepancy appears to change sign as a function of Froude number. It would be interesting to test lenticular ship models and compare measured wave resistance with the wave resistances of $\sigma_M(x)$ and $\sigma_{EIF}(x)$**. It would be significant and useful if a consistently better agreement were found using $\sigma_{EIF}(x)$.

---

* Typical values of ϵ are .04 for a destroyer, .048 for a tanker, based on the waterplane section.

** All modified for finite draft.

The results derived above for a special class of forms can be used to construct new dipole distributions for general forms having a finite entrance angle. This can be done at each depth in an ad hoc fashion by multiplying Michell's dipole distribution by $f_{\epsilon(y)}(x)/g_{\epsilon(y)}(x)$, where $\epsilon(y)$ defines the lenticular cylinder having the same entrance angle as the given form at the depth y. This modification, if applied to forms for which model resistance data are already available, would make possible the evaluation of a potential improvement in wave resistance calculation procedures without performing additional model tests.

σ_M and σ_{EIF} predict different asymptotic behaviour of the wave resistance at low speed. It would be interesting to conduct model tests on lenticular struts to evaluate the relative merits of the two theories. However, if we assume that the behaviour of the dipole density at bow and stern at the surface is the same, for an arbitrary form, as for a lenticular cylinder having the same included angle, then the low-speed asymptotic behaviour, which depends only on certain derivatives evaluated at the bow and stern at the surface ([3], [7]), is easily derived in either theory, allowing comparison of the theories with existing experimental results.

Incidentally, it can be seen that σ_{EIF} cannot be used indiscriminately since it predicts infinite wave resistance for a vertical circular cylinder. The theoretical implications of this divergence are being studied. The possibilities of practical application of both σ_M and σ_{EIF} are presumably limited to bodies which more nearly resemble a ship than a verticle circular cylinder does.

APPENDIX A

CONVERGENCE OF THE SERIES FOR $g_\epsilon(x)$ and $f_\epsilon(x)$ AS FUNCTIONS OF ϵ

If we let $p = 2-s$, then from Equation (5)

$$(A\text{-}1) \qquad \epsilon = \frac{s\pi - \sin s\pi}{8 \sin^2 \frac{s\pi}{2}}$$

$$= \frac{\pi s}{12} \left[1 + \frac{(\pi s)^2}{30} + \cdots\right]$$

For thin cylinders, when $2 \geq p > 1$, we have $0 \leq s < 1$, and $0 \leq \epsilon < \pi/8$.

Let us now regard s as a complex variable. The function $\csc \frac{\pi s}{2}$ has simple poles at $s = 0, \pm 2, \pm 4, \cdots$, but at $s = 0$ we have $\epsilon = 0$; thus ϵ is an analytic function of s for $|s| < 1$, the region we are interested in.

Now consider $g_\epsilon(x)$.

$$(A\text{-}2) \qquad g_\epsilon(x) = \frac{1}{2} \left(\sqrt{\cot^2 \frac{\pi s}{2} + 1 - 4x^2} - \cot \frac{\pi s}{2}\right)$$

The function $\cot \frac{\pi s}{2}$ has simple poles at $s = 0, \pm 2, \cdots$, but at $s = 0$ we have $g_\epsilon(x) = 0$. The square root $\sqrt{\cot^2 \frac{\pi s}{2} + 1 - 4x^2}$ has a branch point when $s = s_o$, where $\cot^2 \frac{\pi s_o}{2} = -(1-4x^2)$, or $s_o = 1 \pm 2n + \frac{2}{\pi} \operatorname{Arctan} (i \sqrt{1-4x^2})$, $n = 0, 1, 2, \cdots$

Thus $|s_o| \geq 1$, and $g_\epsilon(x)$ is an analytic function of s for $|s| < 1$

Now consider $f_\epsilon(x)$. Let $R = \frac{1+2x}{1-2x}$, then

$$f_\epsilon(x) = \frac{\frac{1}{2-s} \sin \frac{2\pi}{2-s}}{\cosh \left[\frac{2}{2-s} \ln R\right] - \cos \frac{2\pi}{2-s}} \tag{A-3}$$

The denominator of Eq. (A-3) becomes zero when $s = s_1$, and

$$s_1 = \frac{\pi(1 + 2n) - i \ln R}{n\pi} \qquad n = 0, 1, 2, \cdots$$

Thus $|s_1| \geq 1$, and $f_\epsilon(x)$ is an analytic function of s for $|s| < 1$.

Therefore, both $g_\epsilon(x)$ and $f_\epsilon(x)$ can be expressed as a convergent power series in s for $0 \leq s < 1$.

For $s \to 0$, $\epsilon \to 0$, s and ϵ are linearly related (see Equation (A-1)), and hence if a convergent power series expansion exists in powers of s, such an expansion also exists in powers of ϵ.

APPENDIX B

RELATIONS BETWEEN NORMALIZED AND UNNORMALIZED QUANTITIES

Let $\hat{g}_\epsilon(\hat{x})$ define a lenticular cylinder of length L via

$$\hat{z} = \pm\, \hat{g}_\epsilon(\hat{x}),$$

where ϵL is average half-beam. If we let $\hat{z} = zL$, $\hat{y} = yL$, $\hat{x} = xL$ and define $g_\epsilon(x) = L^{-1}\hat{g}_\epsilon(xL)$ we find

$$z = \pm\, g_\epsilon(x)$$

as the normalized form of the lenticular cylinder. If

$$\hat{\phi}_\epsilon(\hat{x},\hat{z}) + c\hat{x}$$

is the total potential describing a uniform flow past a lenticular cylinder in unnormalized coordinates, and if we let $\hat{\phi}_\epsilon(xL,\ zL) = \phi_\epsilon(x,z)$ we find that the total normalized potential is

$$\phi_\epsilon(x,z) + cLx.$$

The linearized relation

$$\frac{\partial \hat{\phi}_\epsilon(\hat{x}, o \pm)}{\partial \hat{z}} = \pm\, c\, \frac{d\hat{g}_\epsilon(\hat{x})}{d\hat{x}}$$

becomes

$$\frac{\partial \phi_\epsilon(x, o \pm)}{\partial z} = \pm\, c\, \frac{dg_\epsilon(x)}{dx}$$

in normalized coordinates. Since the dipole density is

$-\frac{1}{2\pi}\int^{\hat{x}} \frac{\partial \hat{\phi}_\epsilon(\hat{x}, o^+)}{\partial \hat{z}}\, d\hat{x}$ we have the following linearized relations:

Unnormalized dipole density = $-\frac{c}{2\pi}\hat{g}_{\epsilon}(\hat{x})$

Normalized dipole density = $-\frac{c}{2\pi}g_{\epsilon}(x)$.

For completeness we note that the free surface condition in normalized coordinates is

$$\frac{\partial^2 \phi}{\partial x^2} = F\frac{\partial \phi}{\partial y}, (y = 0)$$

where $F = \frac{gL}{c^2}$.

APPENDIX C.

SUPERCIRCULAR CYLINDERS, $0 \leq p \leq 1$

Consider the velocity potential $\hat{\phi}$ as given by Equation (4): $\hat{\phi}$ becomes infinite whenever $\eta = 0$ and $\xi = mp\pi$, where $m = 1, 2, 3, \cdots$. Since in the region of interest, $\hat{z} \geq 0$, we must have $0 \leq \xi \leq \pi$, the restriction on m is

(C-1) $\quad mp \leq 1$.

Therefore, for $p>1$ (subcircular cylinders) no m satisfies Equation (C-1). For supercircular cylinders, $p = p_o \leq 1$, there are m_o singularities in ϕ, where m_o is the largest integer satisfying the equation $m \leq 1/p_o$.

The rectangular coordinates corresponding to $\eta = 0$ and $\xi = mp\pi$ are

$$\hat{x}_m = 0$$

(C-2)

$$\hat{z}_m = \frac{a \sin mp\pi}{1-\cos mp\pi}$$

Note that the point $(0,\hat{z}_m)$ for $m \geq 1$ is inside the cylinder because $\xi = mp\pi > \xi_o = \frac{p\pi}{2}$.

Let us define local polar coordinates r, α with origin at $(0, \hat{z}_m)$, see Figure 11. As $\eta \to 0$ and $\xi \to mp\pi$ Equation (4) can be written as

(C-3) $$\hat{\phi}_m \to 2ca \frac{\eta}{\eta^2+(mp\pi-\xi)^2}$$

which in terms of r and α for $r \ll 1$ becomes

$$\hat{\phi}_m \to \mu_m \frac{\cos\alpha}{r} \tag{C-4}$$

where

$$\mu_m = \frac{2ca^2}{1-\cos mp\pi} \tag{C-5}$$

Equation (C-4) is the potential due to a line dipole source. For p = 1 (circular cylinder) m = 1 and $\mu_1 = ca^2$, $z_1 = 0$, which just expresses the well known fact that a circular cylinder of radius a can be generated in a uniform flow with velocity c by a dipole distribution of strength $\mu_1 = ca^2$ on the axis of the cylinder.

Thus for $p < 1$ in addition to any dipole density - $\frac{c}{2\pi} f_\epsilon(x)$ on the x-axis we also have discrete dipole sources of strength μ_m at $(0, z_m)$. As p decreases, z_m for a given m increases, and so does μ_m; also new discrete dipoles are created at the origin as p decreases (whenever $p = \frac{1}{m}$ for some m), which then split and move away from the origin in the negative and positive z-directions as p decreases further.

So far we have kept the length 2a constant, which means that the circles forming the cross section increase as $p \to 0$. Now let us keep the radius k of the circles constant, in which case 2a decreases as $p \to 0$,

$$a = k \sin \frac{p\pi}{2} \tag{C-6}$$

Equations (C-2) and (C-5) become

$$\hat{z}_m = k \frac{\sin \frac{p\pi}{2} \sin mp\pi}{1-\cos mp\pi} \tag{C-7}$$

$$\mu_m = 2ck^2 \frac{\sin^2 \frac{p\pi}{2}}{1-\cos mp\pi} \tag{C-8}$$

If we now let $p \to 0$ while k remains constant, the circles become tangent at the origin, and there is an infinite number of discrete dipoles on the z-axis at

$$\hat{z}_m = \frac{k}{m}, \qquad m = 1, 2, 3, \cdots \tag{C-9}$$

of strength

$$\mu_m = \frac{ck^2}{m^2} \tag{C-10}$$

Note that z_m never exceeds k, and the strength of the dipoles near the origin approaches zero.

BIBLIOGRAPHY

[1] J.H. Michell, The Wave Resistance of a Ship; Phil. Mag., Vol. 45, p. 106, 1898.

[2] J.J. Stoker, A.S. Peters, The Motion of a Ship, as a Floating Rigid Body, in a Seaway, Communications on Pure & Applied Math., 1957, Vol. 10, Issue 3, pp. 399-490.

[3] J.V. Wehausen, Wave Resistance of Thin Ships, Proc. Symp. Naval Hydrodynamics, Publ. 515, Nat. Acad. Sciences - Nat. Res. Council, pp. 109-137, 1957.

[4] L.M. Milne-Thomson, Theoretical Hydrodynamics, 3rd ed., The MacMillan Co., 1955, p. 169.

[5] S. Karp, J. Kotik, and J. Lurye, On the Problem of Minimum Wave Resistance for Struts and Strut-Like Dipole Distributions, 3rd Symposium on Naval Hydrodynamics in Scheveningen (The Hague), Netherlands, Sep. 1960.

[6] L. Landweber and C.S. Yih, Forces, Moments, and Added Masses for Rankine Bodies, J. Fluid Mech., Vol. 1, p. 319, 1956.

[7] J. Kotik, The Asymptotic Expansion of Michell's Integral For Low Froude Number, Unpublished.

SUPPLEMENTARY REFERENCES

[8] J.K. Lunde, The Linearized Theory of Wave Resistance and its Application to Ship-Shaped Bodies in Motion on the Surface of a Deep, Previously Undisturbed Fluid, Techn. & Res. Bull. No. 1-18, Soc. Naval Arch. & Marine Eng., New York, N.Y., July 1957.

[9] K. Eggers, W. Wetterling, Ueber die Ermittlung der schiffsaehnlichen Umstroemungskoerper vorgegebener Quell-Senken-Verteilungen mit Hilfe Elektronischer Rechenmaschinen, Schiffstechnik, Vol. 45, p. 284, 1957.

[10] H. Amtsberg, Beitrag Zur Frage des Rauhigkeitseinflusses auf den Schiffwiderstand, Schiffbautechnischen Gessellschaft, Vol. 38, p. 135, 1937.

[11] H. Munk, Lectures in Aerodynamics at the Catholic University of America, Aerodynamics [edited by Durand], Vol. 1, pp. 224-304.

[12] L. Landweber, The Axially Symmetric Potential Flow About Elongated Bodies of Revolution, David Taylor Model Basin, Report (761), 1951.

[13] W. Cummins, Forces and Moments on Submerged Bodies Moving Under Waves, Proc. of the First Conference on Ships and Waves, p. 207, 1954.

[14] D.W. Taylor, On Solid Stream Forms and the Depth of Water Necessary to Avoid Abnormal Resistance of Ships, Transactions of the Institution of Naval Architects, Vol. 35, p. 234, 1895.

[15] T. Inui, A New Theory of Wave-making Resistance, Based on the Exact Conditions of the Surface of Ships, J. Soc. Naval Architects, Japan, Vol. 85, pp. 29-43, Dec. 1952, and Vol. 93, p. 11, July 1953.

[16] H.L. Pond, The Moment Acting on a Ranking Ovoid Moving Under a Free Surface, J. Ship Res., Vol. 2, No. 4, p. 1, March 1959.

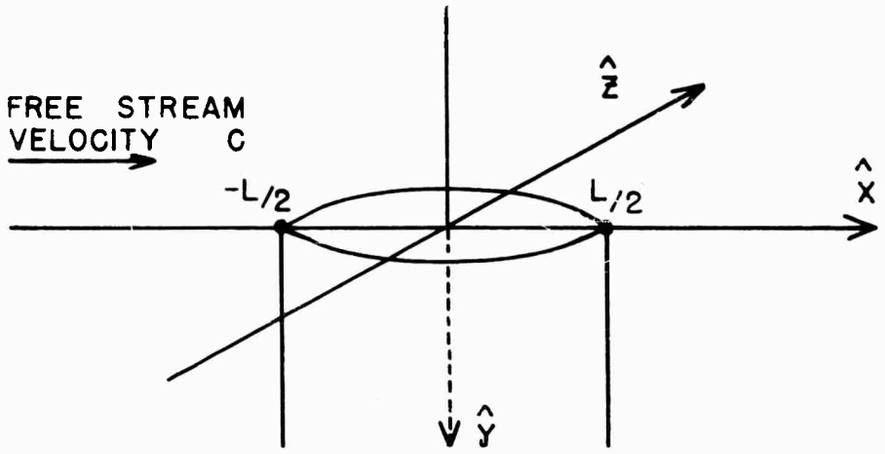

FIGURE 1A
LENTICULAR CYLINDER IN A SEMI—INFINITE FLUID,
UNNORMALIZED COORDINATES

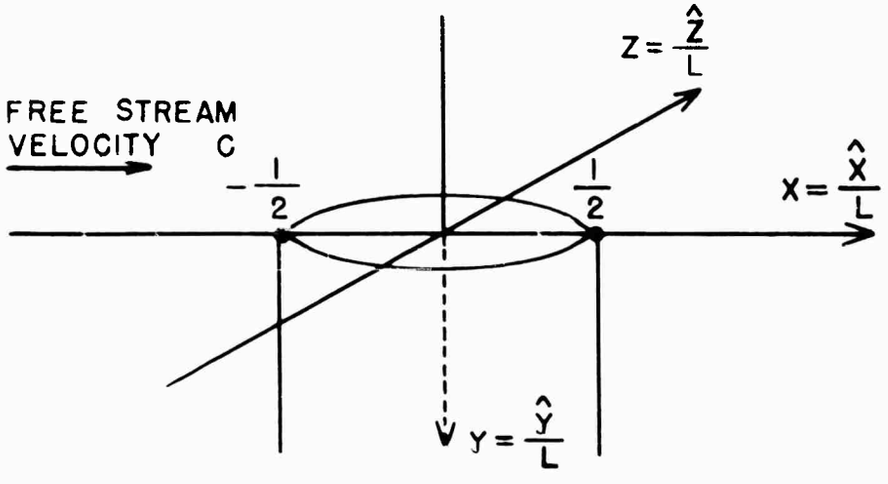

FIGURE 1B
LENTICULAR CYLINDER IN A SEMI—INFINITE FLUID,
NORMALIZED COORDINATES

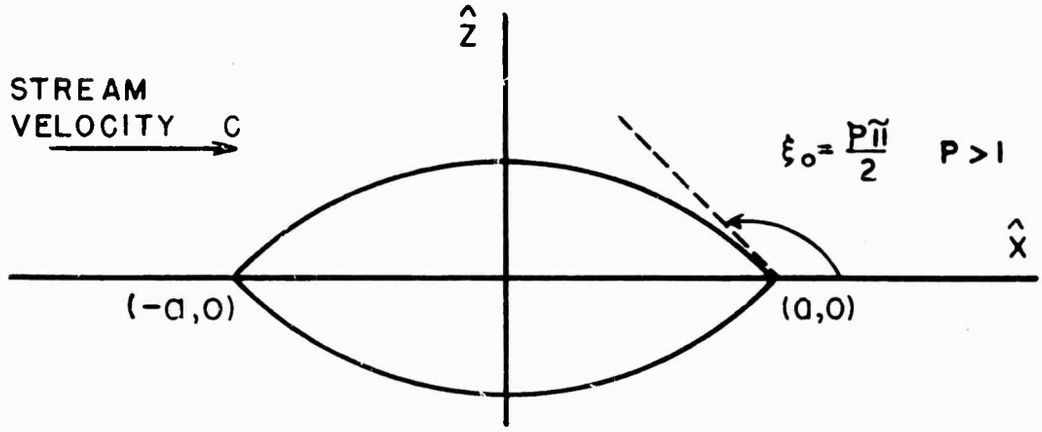

FIG. 2A
SUBCIRCULAR LENTICULAR CYLINDER

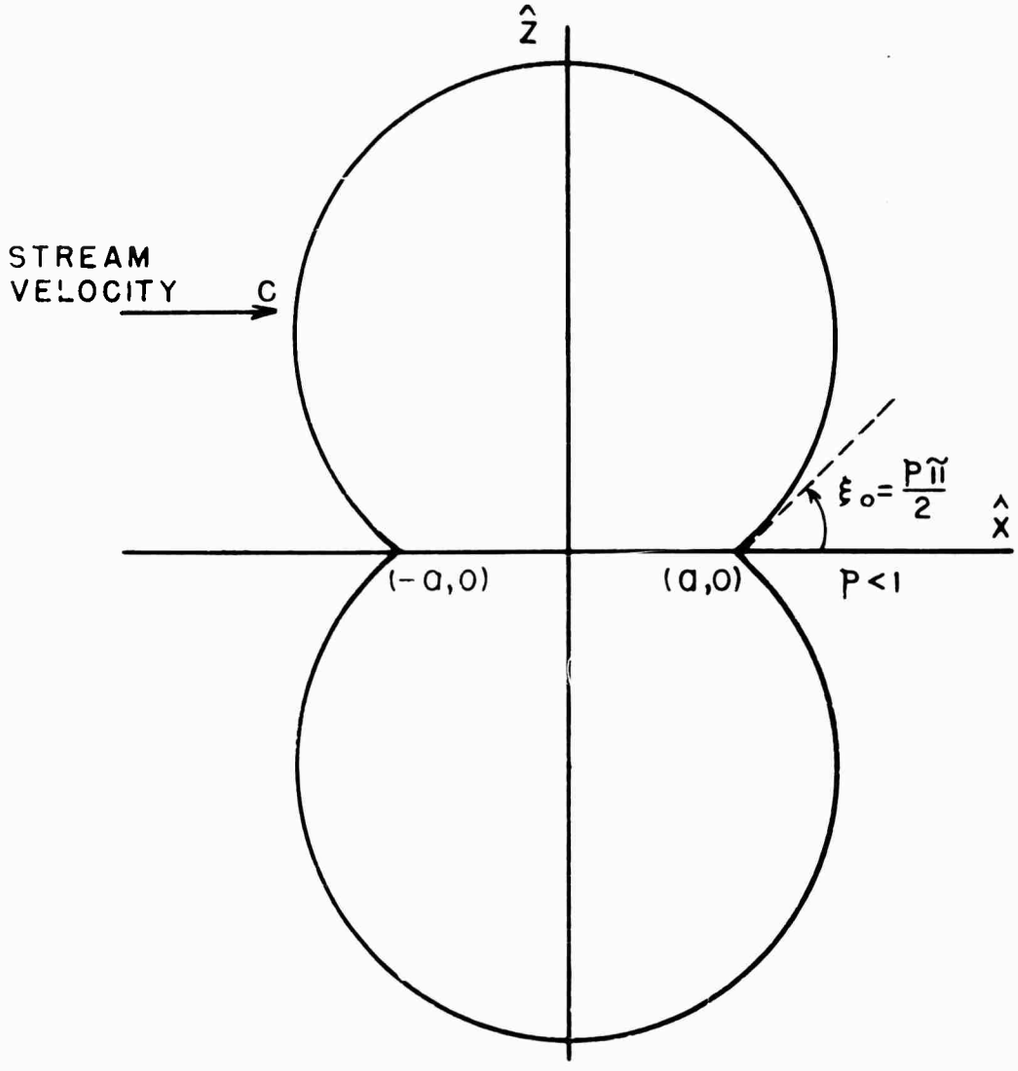

FIG. 2B
SUPERCIRCULAR LENTICULAR CYLINDER

FIG. 3

FULLNESS PARAMETER ϵ VS. ANGULAR PARAMETER P

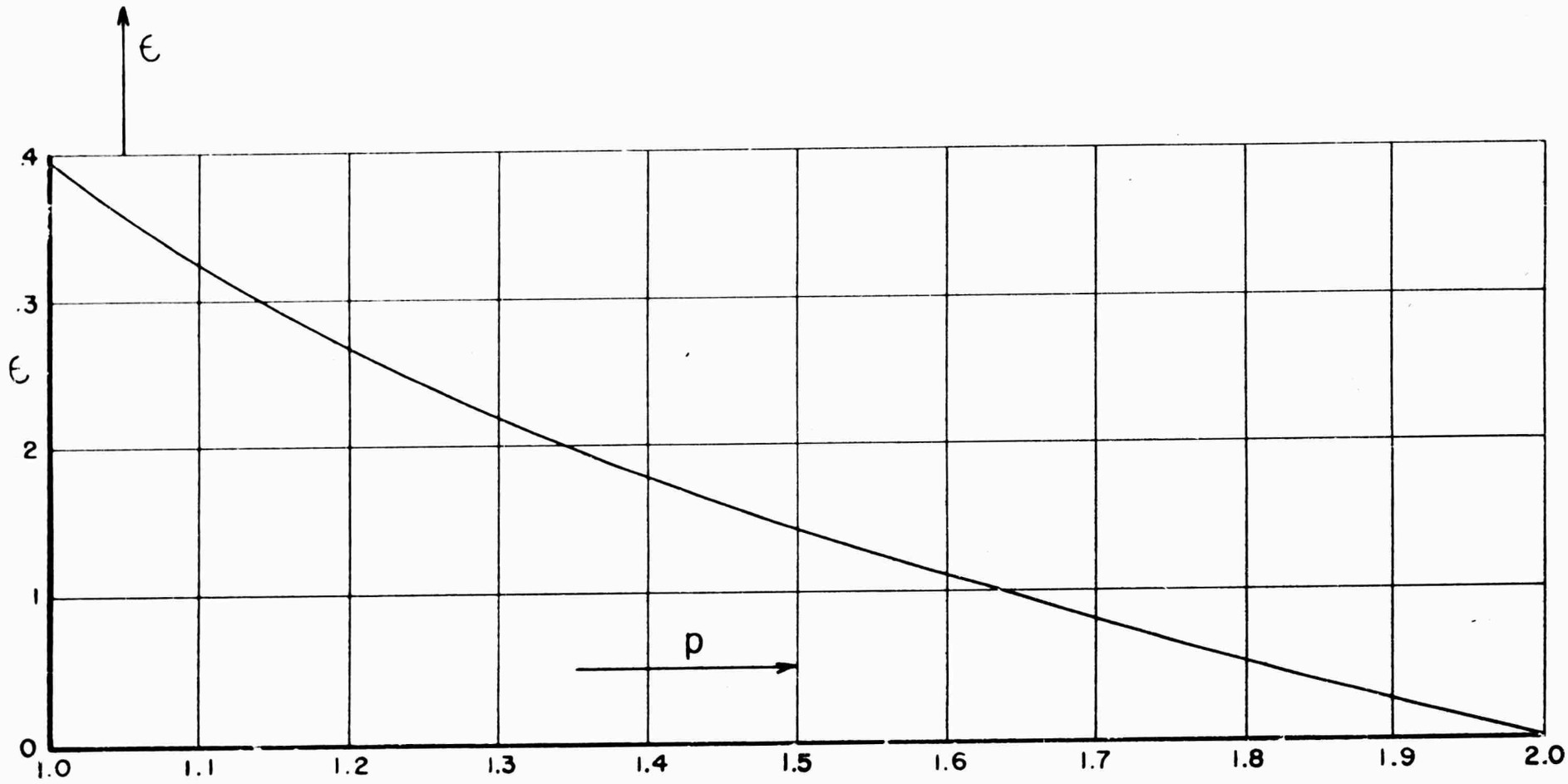

FIG. 4

$f_\epsilon(x)$ and $g_\epsilon(x)$ vs. x

for $\epsilon = .025$

$p = 1.905$

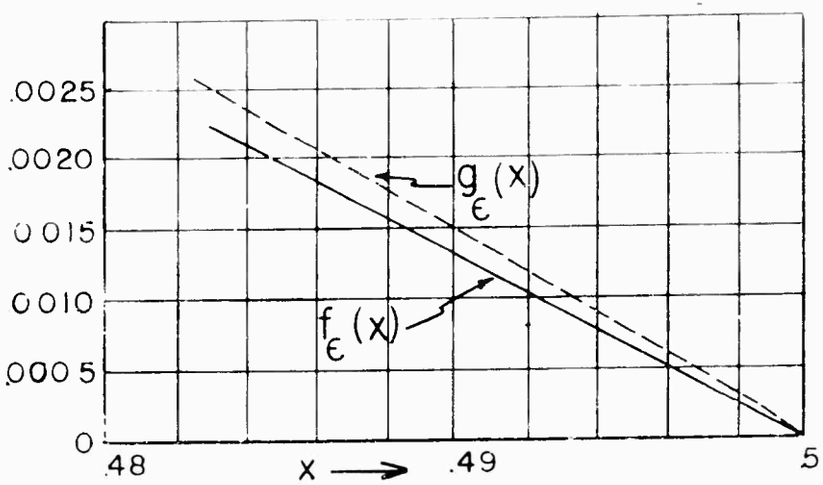

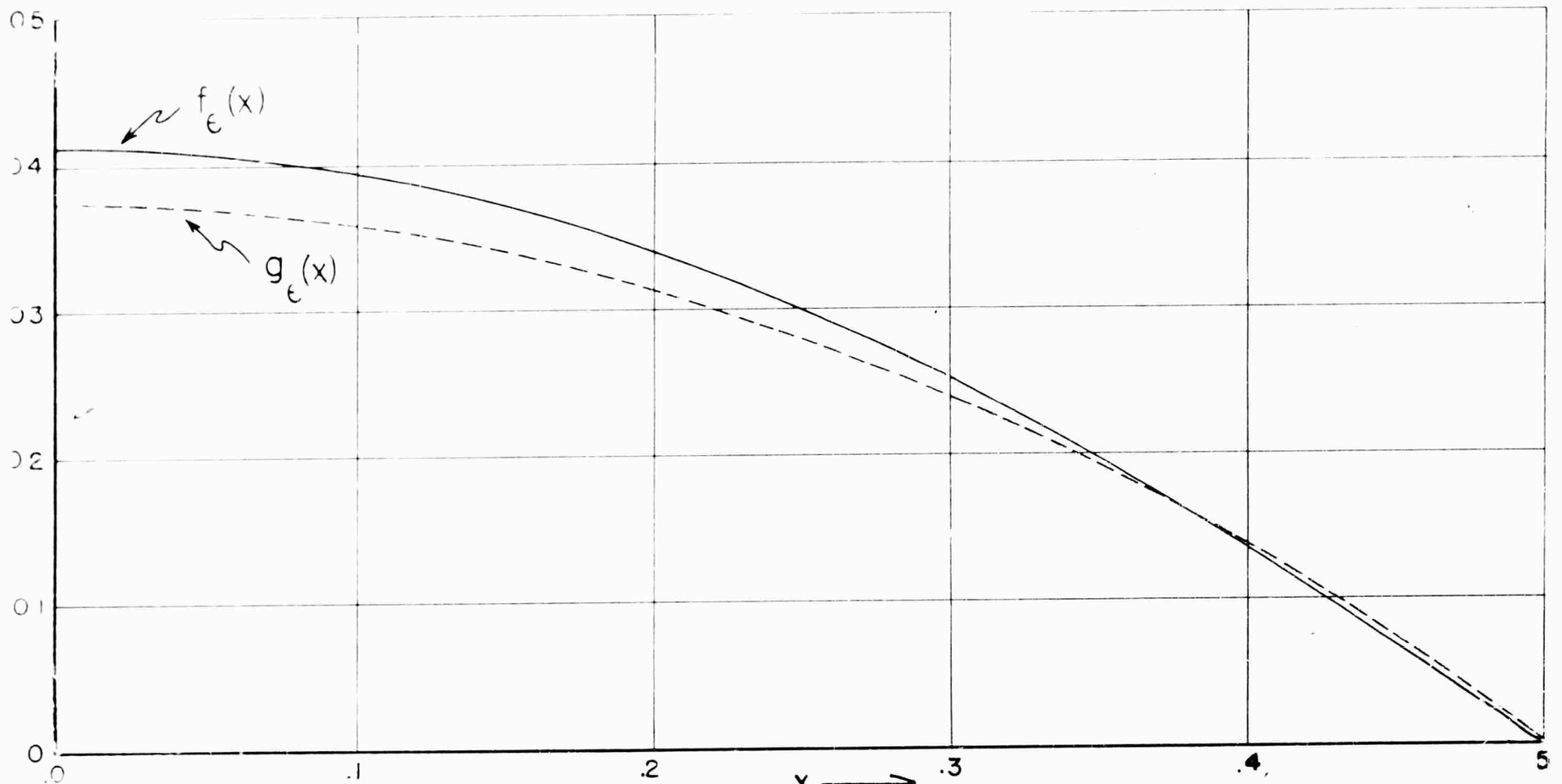

FIG. 5

$f_\epsilon(x)$ and $g_\epsilon(x)$ vs. x

for $\epsilon = .05$

$p = 1.812$

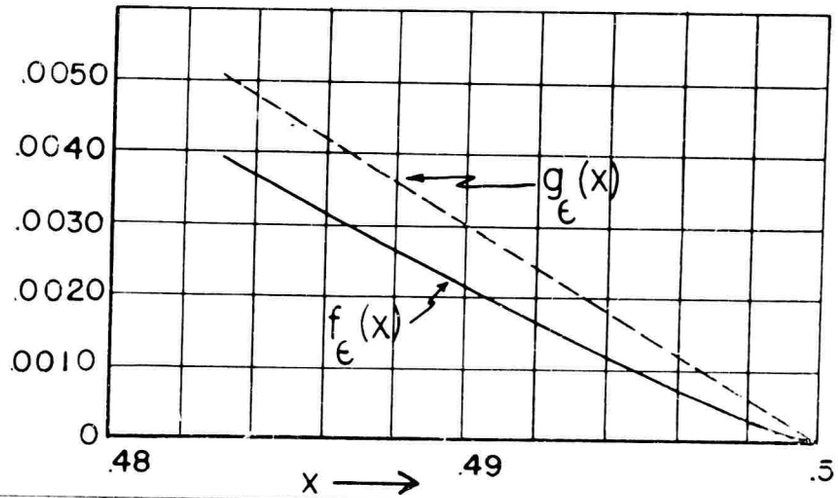

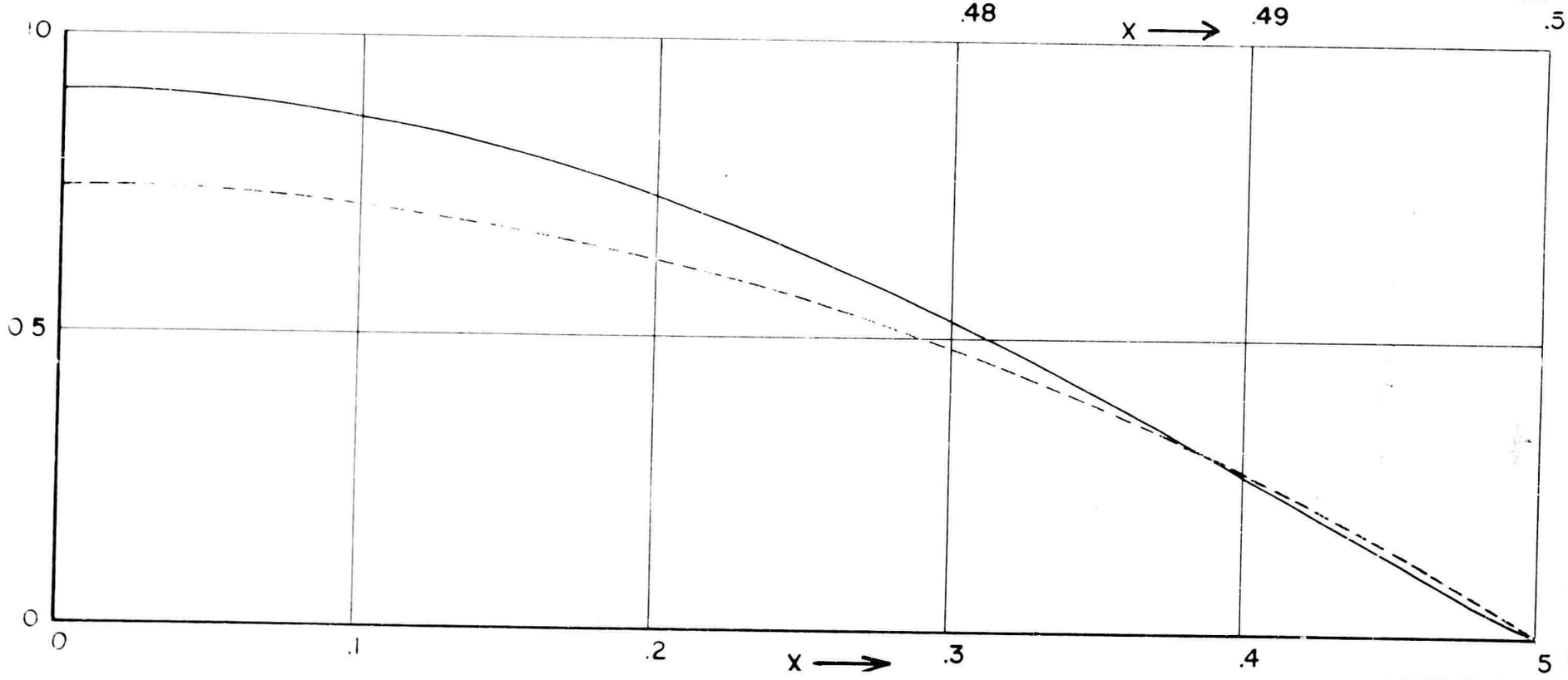

FIG. 6

$f_\epsilon(x)$ and $g_\epsilon(x)$ vs x

for $\epsilon = .10$

$p = 1.635$

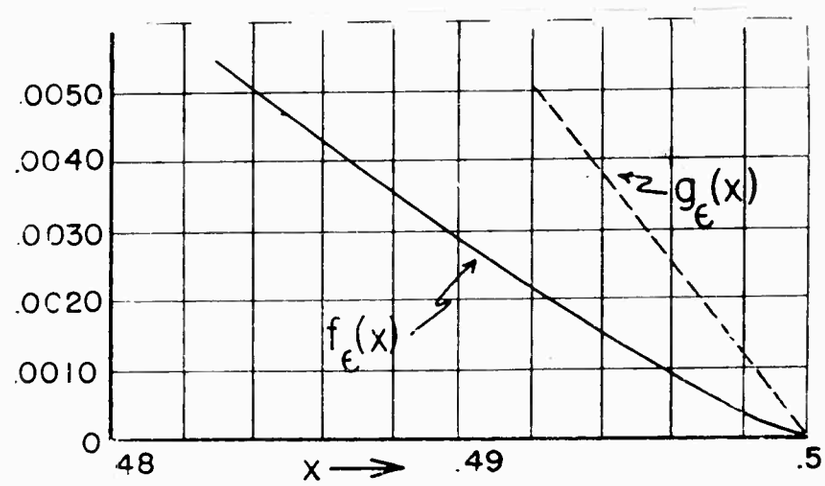

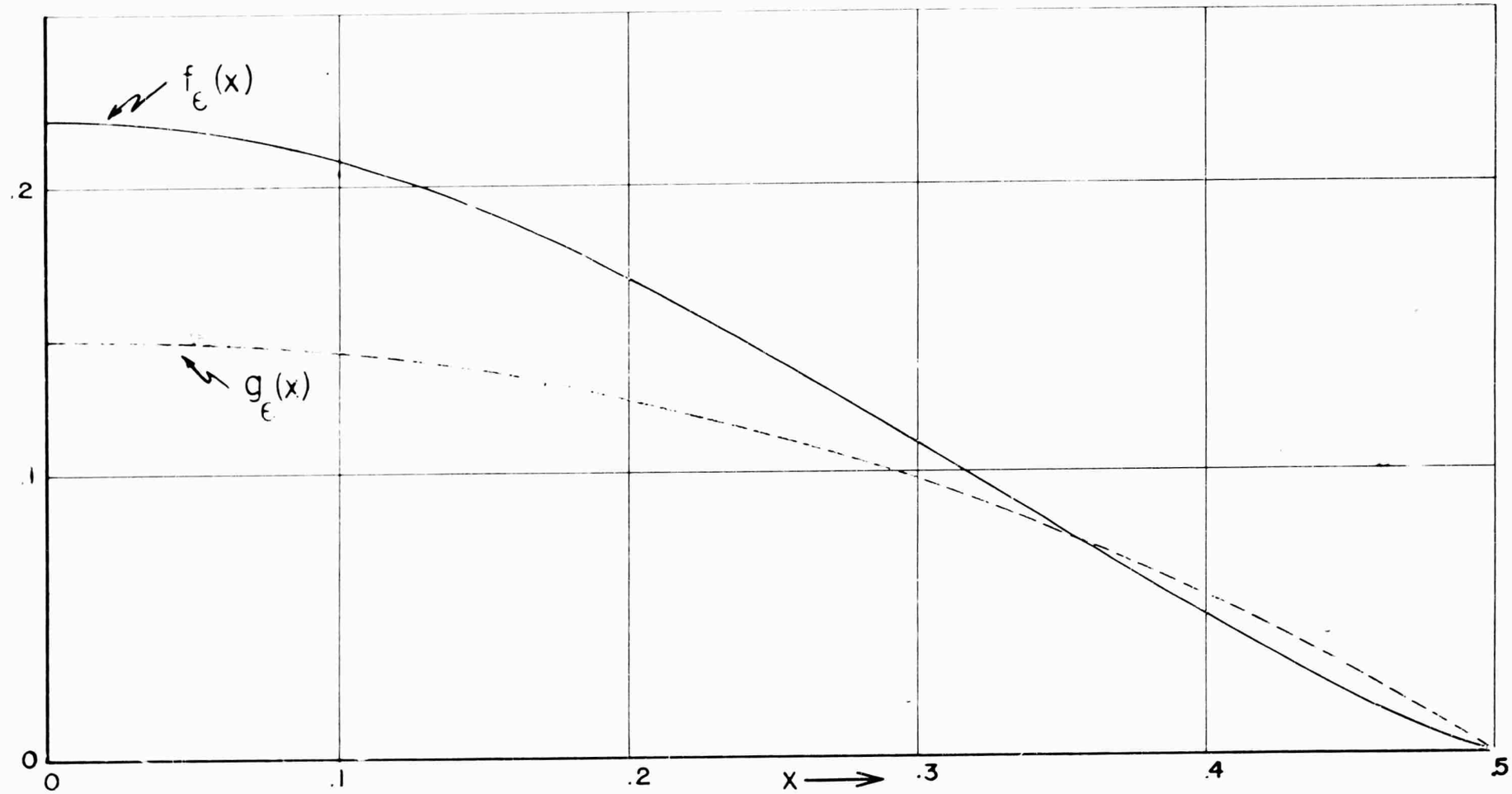

FIG. 7

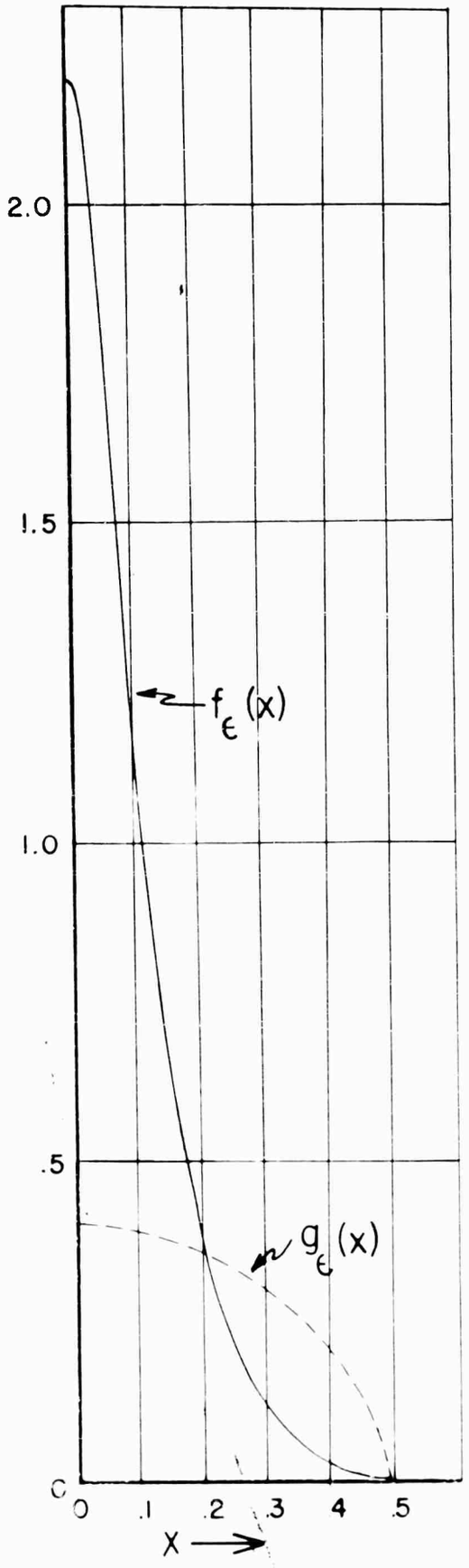

$f_\epsilon(x)$ and $g_\epsilon(x)$ vs. x

for $\epsilon = .3$

$p = 1.138$

FIG. 8

$\epsilon_g^2 C_w^M$ and $\epsilon_f^2 C_w^{EIF}$ vs. Froude number

for p = 1.905

ϵ_g = .025

ϵ_f = .027

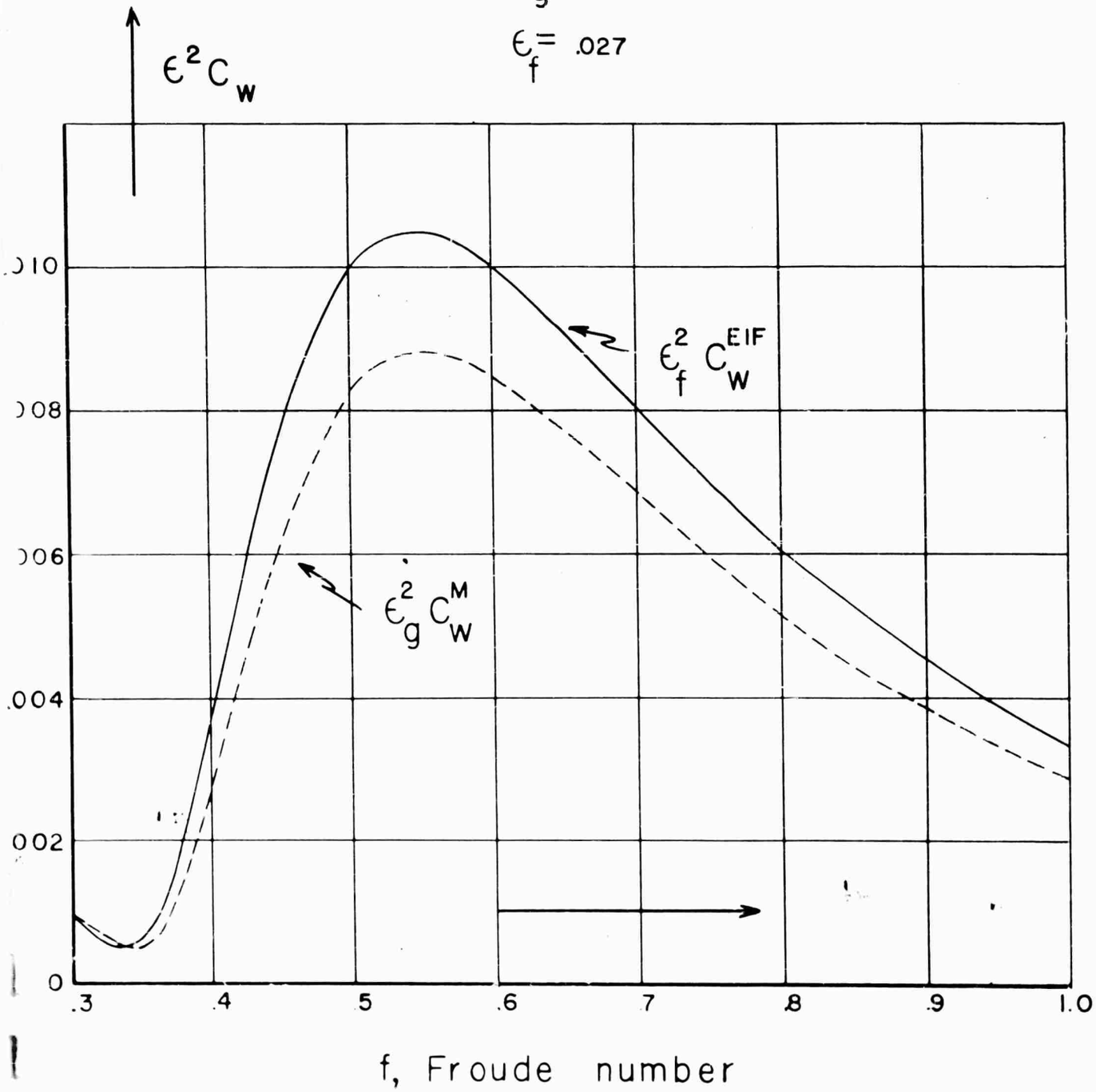

FIG. 9

$\epsilon_g^2 C_w^M$ and $\epsilon_f^2 C_w^{EIF}$ vs. Froude number

for $p = 1.812$

$\epsilon_g = .050$

$\epsilon_f = .057$

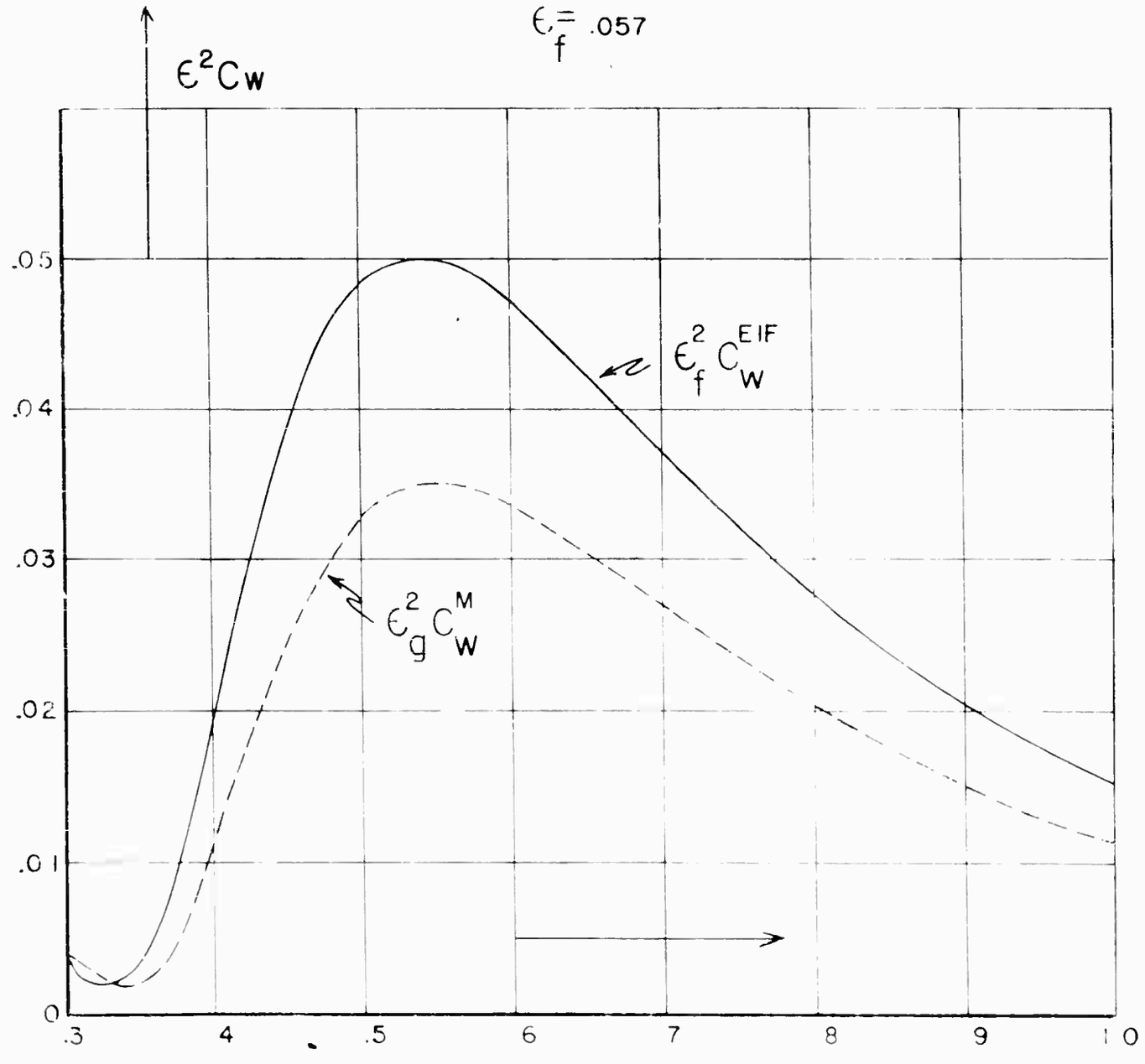

$\epsilon_g^2 C_w^M$ and $\epsilon_f^2 C_w$ vs. Froude number

for $p = 1.635$

$\epsilon_g = .100$

$\epsilon_f = .130$

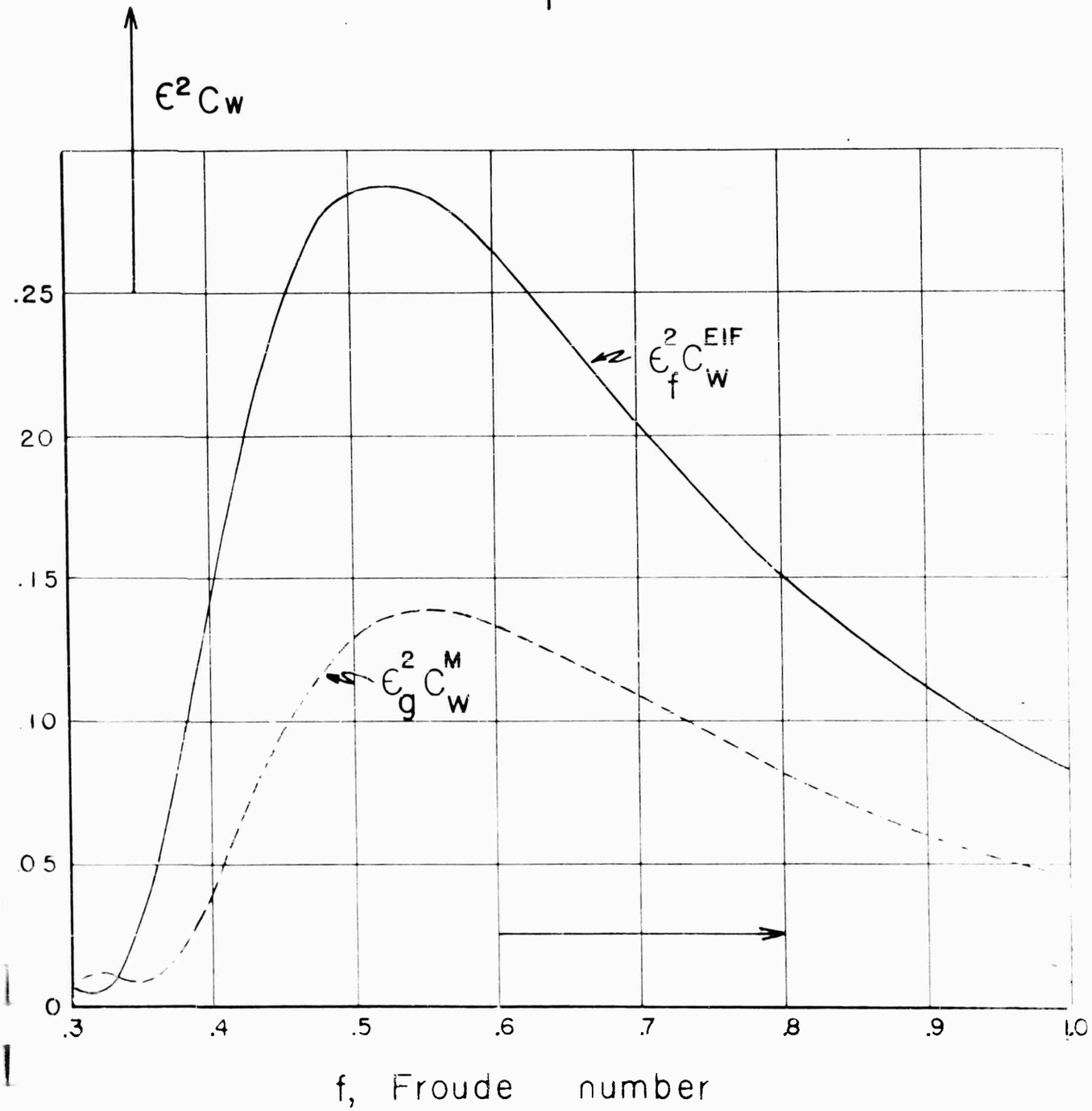

FIG. 10

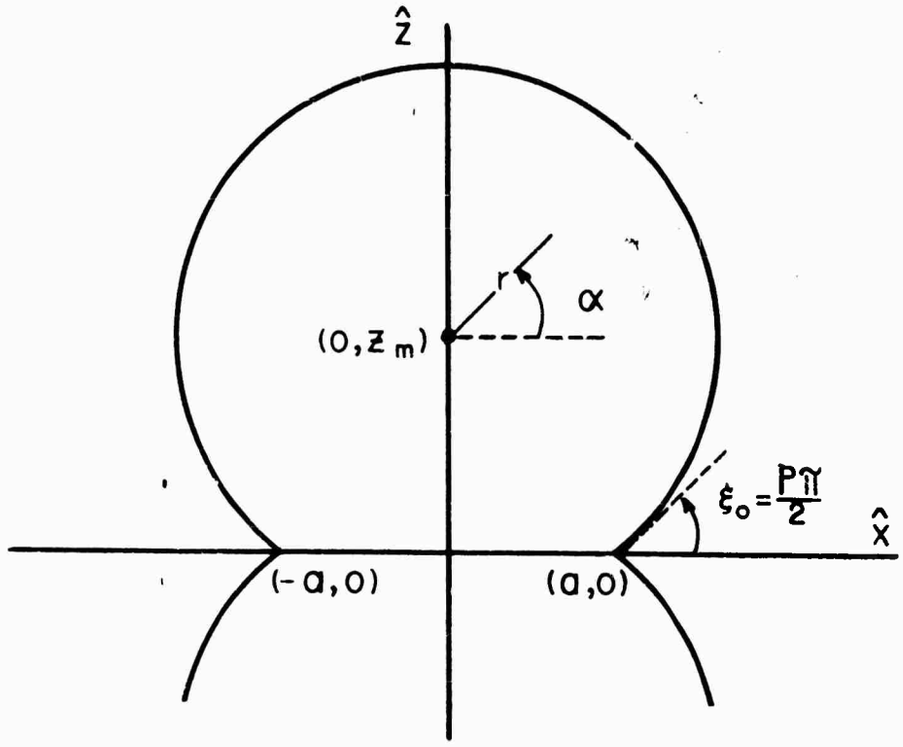

FIG. 11
LOCAL COORDINATES FOR A
SINGULARITY IN A SUPERCIRCULAR CYLINDER

DISTRIBUTION LIST FOR UNCLASSIFIED TECHNICAL
REPORTS ON CONTRACT Nonr-2427(00)

Chief of Naval Research
Department of the Navy
Washington 25, D.C.
Attn: Code 438 (2)

Commanding Officer
Office of Naval Research
Branch Office
The John Crerar Library
Building
86 East Randolph Street
Chicago 1, Illinois (1)

Commanding Officer
Office of Naval Research
Branch Office
346 Broadway
New York 13, New York (1)

Commanding Officer
Office of Naval Research
Branch Office
1030 East Green Street
Pasadena 1, California (1)

Commanding Officer
Office of Naval Research
Branch Office
1000 Geary Street
San Francisco 9, California (1)

Commanding Officer
Office of Naval Research
Branch Office
Navy No. 100,
Fleet Post Office
New York, New York (25)

Director
Naval Research Laboratory
Washington 25, D.C.
Attn: Code 2021 (Library) (6)

Chief, Bureau of Aeronautics
Department of the Navy
Washington 25, D.C.
Attn: Codes AD-3(Aero & Hydro Branch) (1)
RS (Research Division) (1)

Chief, Bureau of Ordnance
Department of the Navy
Washington 25, D.C.
Attn: Codes RE(Ass't. Chief for R & D) (1)
SP26(Ship Installation Branch) (1)

Chief Bureau of Ships
Department of the Navy
Washington 25, D.C.
Attn: Codes 106 (Tech. Ass't to Chief of Bureau) (1)
310 (Research & Development Division) (1)
312 (Technical Library) (1)
420 (Preliminary Design Branch) (1)
421 (Preliminary Design Section) (1)
440 (Hull Design Branch) (1)
442 (Scientific and Research) (1)

Chief, Bureau of Yards and Docks
Department of the Navy
Washington 25, D.C
Attn: Code D-400
(Research Division) (1)

Commander
Military Sea Transportation
Service
Department of the Navy
Washington 25, D.C. (1)

Commanding Officer & Director
David Taylor Model Basin
Washington 7, D.C.
Attn: Codes 142
(Library Branch) (1)
500 (Technical
Director for Hydromechanics
Lab.) (1)
513 (Contract
Research Administrator) (1)
580 (Seaworthiness & Fluid Dynamics Div.) (1)

Commander
U.S. Naval Ordnance Test Station
China Lake, California
Attn: Code 753 (Library Div.) (1)

Superintendent
U.S. Naval Postgraduate School
Monterey, California (1)

Commander
Portsmouth Naval Shipyard
Portsmouth, New Hampshire (1)

Commander
Norfolk Naval Shipyard
Portsmouth, Virginia (1)

Commander
Boston Naval Shipyard
Boston, Massachusetts (1)

Commander
Naval Proving Ground
Dahlgren, Virginia (1)

Commander
Pearl Harbor Naval Shipyard
Navy No. 128,
Fleet Post Office
San Francisco, California (1)

Commander
San Francisco Naval Shipyard
San Francisco, California (1)

Commander
Mare Island Naval Shipyard
Vallejo, California
Attn: Shipyard Technical Library
Building 746, Code 370a (1)

Commander
New York Naval Shipyard
Brooklyn, New York (1)

Commander
Puget Sound Naval Shipyard
Bremerton, Washington (1)

Commander
Philadelphia Naval Shipyard
Philadelphia, Pennsylvania (1)

Commander
Charleston Naval Shipyard
Charleston, South Carolina (1)

Commander
Long Beach Naval Shipyard
Long Beach, California (1)

Dr. A.V. Hershey
Computation & Exterior Ballistics Lab.
U.S. Naval Proving Ground
Dahlgren, Virginia (1)

Commandant
U.S. Coast Guard
1300 E. Street, N.W.
Washington, D.C. (1)

Secretary, Ship Structure Committee
U.S. Coast Guard Headquarters
1300 E. Street, N.W.
Washington 25, D.C. (1)

Superintendent
U.S. Naval Academy
Annapolis, Maryland
Attn: Library (1)

Maritime Administration
441 G Street, N.W.
Washington, D.C.
Attn: Division of Ship Design,
Mr. Vito L. Russo (1)

Superintendent
U.S. Merchant Marine Academy
Kings Point, Long Island, New York
Attn: Capt. L.S. McCready, Head
Dept. of Engineering (1)

U.S. Army Transportation Research
& Development Command
Fort Eustis, Virginia
Attn: Marine Transport Div. (1)

Director of Research
National Aeronautics & Space
Administration
1512 H Street, N.W.
Washington 25, D.C. (1)

M. J.B. Parkinson
Langley Aeronautical Laboratory
National Aeronautics & Space
Administration
Langley Field, Virginia (1)

Director
Engineering Sciences Division
National Science Foundation
1520 H Street, N.W.
Washington, D.C. (1)

Director
National Bureau of Standards
Washington 25, D.C.
Attn: Fluid Mechanics Div.
Dr. G.B. Schubauer (1)
Dr. G.H. Keulegan (1)

Document Service Center
Armed Services Technical
Information Agency
Arlington Hall Station
Arlington 12, Virginia (5)

Office of Technical Services
Department of Commerce
Washington 25, D.C. (1)

California Institute of Technology
Pasadena 4, California
Attn: Prof. C.B. Millikan (1)
Prof. T.Y. Wu (1)

University of California
Berkeley 4, California
Attn: Department of Engineering
Prof. H.A. Schade (1)
Prof. J. Johnson (1)
Prof. J.V. Wehausen (1)

Director
Scripps Institute of Oceanography
University of California
La Jolla, California (1)

Prof. M. Albertson
Department of Civil Engineering
Colorado A & M College
Fort Collins, Colorado (1)

Iowa Institute of Hydraulic Research
State University of Iowa
Iowa City, Iowa
Attn: Prof. H. Rouse, Director (1)
Prof. L. Landweber (2)

Harvard University
Cambridge 38, Massachusetts
Attn: Prof. G. Birkhoff,
Dept. of Math. (1)
Prof. G.F. Carrier,
Dept. of Engrg. Sci. (1)

Department of Naval Architecture
& Marine Engineering
Massachusetts Institute of Technology
Cambridge 39, Massachusetts
Attn: Prof. L. Troost (1)
Prof. P. Mandel (1)

Professor R.B. Couch
Department of Naval Architecture
University of Michigan
Ann Arbor, Michigan (1)

Director
St. Anthony Falls Hydraulic Lab.
University of Minnesota
Minneapolis 14, Minnesota (1)

Institute of Mathematical Science
New York University
25 Waverly Place
New York 3, New York
Attn: Prof. J.J. Stoker (1)
Prof. A. Peters (1)
Prof. J. Keller (1)

Professor W.J. Pierson, Jr.
Department of Oceanography
New York University
University Heights
New York 53, New York (1)

Professor J.J. Foody
Engineering Department
New York State University
Maritime College
Fort Schulyer, New York (1)

Director
Ordnance Research Laboratory
Pennsylvania State University
University Park, Pennsylvania (1)

Technical Library
Webb Institute of Naval Architecture
Crescent Beach Road
Glen Cove, Long Island, New York (1)

Prof. W.R. Sears
Graduate School of Aeronautical Engineering
Cornell University
Ithaca, New York (1)

Director
Woods Hole Oceanographic Institute
Woods Hole, Massachusetts (1)

Society of Naval Architects And Marine Engineers
74 Trinity Place
New York 6, New York (1)

Director
Stevens Institute of Technology
Experimental Towing Tank
711 Hudson Street
Hoboken, New Jersey (2)

National Research Council
Montreal Road
Ottawa 2, Canada
Attn: Mr. E.S. Turner (1)

Therm, Incorporated
Ithaca, New York (1)

Commanding Officer & Director
U.S. Naval Civil Engineering Laboratory
Port Hueneme, California
Attn: Code L54 (1)

Prof. F. Ursell
University of Manchester
Dept. of Mathematics
Manchester 13, England (1)

Hydronautics Incorporated
200 Monroe Street
Rockville, Maryland
Attn: Mr. Philip Eisenberg (1)
Mr. Marshall P. Tulin (1)

Dr. R. Tippan
Dept. of Applied Mathematics
Technological University
Julianalaan 132
Delft, Holland (1)

Dr. K. Eggers
Institut fur Schiffbau
University of Hamburg
Berliner Tor 21
Hamburg, Germany (1)

Prof. R.C. MacCamy
Dept. of Mathematics
Carnegie Institute of Technology
Pittsburgh 10, Pennsylvania (1)

Professor J.E. Cermak
Dept. of Civil Engineering
Colorado State University
Fort Collins, Colorado (1)